Journal of Nonlinear Science (2024) 34:19
https://doi.org/10.1007/s00332-023-09996-w

Journal of Nonlinear Science

Cognitive Consumer-Resource Spatiotemporal Dynamics with Nonlocal Perception

Yongli Song[1] · Hao Wang[2] · Jinfeng Wang[3]

Received: 15 July 2022 / Accepted: 27 October 2023

Abstract

Nonlocal perception is crucial to the mechanistic modeling of cognitive animal movement. We formulate a diffusive consumer-resource model with nonlocal perception on resource availability, where resource dynamics is explicitly modeled, to investigate the influence of nonlocal perception on stability and spatiotemporal patterns. For the finite domain, nonlocal perception described by two common types of resource detection function (spatial average or Green function) has no impact on the stability of the spatially homogeneous steady state. For the infinite domain, nonlocal perception described by the Laplacian or Gaussian detection function has no impact on stability either; however, the top-hat detection function can destabilize the spatially homogeneous steady state when the rate of perceptual movement is large and the detection scale belongs to an appropriate interval. Using the more realistic top-hat perception kernel, we investigate the influence of the detection scale, the perceptual movement rate and the resource's carrying capacity on the spatiotemporal patterns and find the stripe spatial patterns, oscillatory patterns with different spatial profiles as well as spatiotemporal chaos.

Keywords Diffusive consumer-resource dynamics · Nonlocal perception · Detection function · Top-hat kernel · Stability · Spatiotemporal pattern

Mathematics Subject Classification 35B32 · 35B36 · 35K57 · 92B05

Communicated by Dejan Slepcev.

✉ Hao Wang
hao8@ualberta.ca

[1] School of Mathematics, Hangzhou Normal University, Hangzhou 311121, Zhejiang, China

[2] Department of Mathematical and Statistical Sciences, University of Alberta, Edmonton, AB T6G 2G1, Canada

[3] School of Mathematical Sciences, Harbin Normal University, Harbin 150025, Heilongjiang, China

Published online: 18 November 2023

1 Introduction

Animal movement is normally affected by external information including the spatial distribution of resource availability, for example, the smell of pollen. Cognitive movement in response to external information can be characterized by gradient-tracking. Gradient-tracking means that the animal movement tracks the resource gradients, which measures the fastest direction of the growth of the resource. One classical example is the Patlak–Keller–Segel chemotaxis model (Keller and Segel 1971a, b; Patlak 1953). The Patlak–Keller–Segel chemotaxis model provides some initial motivation for how information-based movement models may be constructed and have been extensively studied in the past decades (Carrillo et al. 2020; Hillen and Painter 2009; Tao and Winkler 2012, 2017a, b; Wang et al. 2019). The classical Patlak–Keller–Segel model depends on the gradients of local external information by assuming that bacteria only have a tiny perceptual range. However, nonlocal information, such as visual, auditory, and olfactory cues, plays a vital role in animal movement decisions because animals normally have a large perceptual range (Barnett and Moorcroft 2008; Fagan et al. 2017; Martínez-García et al. 2013; Wang and Salmaniw 2023; Mogilner and Edelstein-Keshet 1999).

The nonlocal information naturally exists and is obtained by an animal's perception. Denote $u(x,t)$ as the density of resources at location x and time t for a one-dimensional infinite landscape and define the forager's resource perception function $h(x,t)$ for the density of resources as

$$h(x,t) = \int_{\Omega} K(x-y)u(y,t)dy, \tag{1.1}$$

where $K(x-y)$ is some reasonable kernel function (also known as the detection function), describing the perception strength of the forager at location x to the resource at location y. The reasonable kernel function $K(x)$ should satisfy the following hypotheses (Wang and Salmaniw 2023): (i) $K(x)$ is symmetric about the origin; (ii) $\int_{\Omega} K(x)dx = 1$; (iii) $\lim_{r\to 0^+} K(x) = \delta(x)$; (iv) $K(x)$ is nonincreasing from the origin. The specific form of the $K(x-y)$ also depends on the boundary condition as is given in Sect. 3. The function h reflects the nonlocal information of resources perceived by foragers. Nonlocal gradient-tracking movements are often used to describe crowd dynamics, flocking or swarming, cell-cell and cell-tissue adhesions; see (Green et al. 2010; Mogilner and Edelstein-Keshet 1999; Grünbaum and Okubo 1994; Börger et al. 2008; Bellomo and Dogbé 2011; Ducrot et al. 2018; Chen et al. 2020; Buttenschøn and Hillen 2021; Giunta et al. 2021) and references therein. The landscapes are called static when the resource distribution $u(x,t)$ is constant in time, and called dynamic otherwise. The issue of how foragers can exploit nonlocal information to improve their success was investigated by Fagan et al. (2017). This study also mentioned that nonlocal gradient-tracking is particularly important in dynamic landscapes, which is the focus of this paper.

Letting $v(x,t)$ denote the density of foragers at location x and time t and assuming that the movement of the foragers follows a perceived nonlocal gradient $(\partial h/\partial x)$,

Fagan et al. (2017) proposed the following nonlocal advection–diffusion equation:

$$v_t = Dv_{xx} - \alpha(vh_x)_x, \tag{1.2}$$

where D and α are the random diffusion and the perception strength, respectively. In Fagan et al. (2017), Eq.(1.2) has been mathematically solved for static resource distributions consisting of one or a sum of sine waves with a top-hat detection function and numerically investigated for the dynamic resource distributions, with the goal of quantifying the effects of the detection-length scale and the random diffusion and the perception strength on foraging success. It has been shown that nonlocal information can be highly beneficial, increasing the spatiotemporal concentration of foragers on their resources up to twofold compared with movement based on purely local information (Fagan et al. 2017).

In Eq.(1.2), the birth/death processes of the forager and the mechanistic dynamics of the resource availability were ignored. Incorporating these important missing pieces into Eq.(1.2), we propose the following consumer-resource model with the nonlocal perception:

$$\begin{cases} u_t = d_1 u_{xx} + f(u, v), & x \in \Omega,\ t > 0, \\ v_t = d_2 v_{xx} - \alpha(vh_x)_x + g(u, v), & x \in \Omega,\ t > 0, \end{cases} \tag{1.3}$$

where Ω is the spatial domain, $\Omega = (0, \ell\pi)$ for the finite domain and $\Omega = (-\infty, +\infty)$ for the infinite domain, $d_1 > 0$ and $d_2 > 0$ are the random diffusion coefficients of the resource and consumer, respectively, $\alpha \geq 0$ is the perceptual diffusion coefficient of the consumer, f and g describe the vital rates of the resource and consumer, respectively, and their interactions. Herbs spread over long distances by means of seed dispersal, which can be considered as the diffusion mechanism of resources. Obviously, (1.3) is more realistic because the resource availability should heavily depend on the consumer's population and feeding rate.

For the biological relevance, we always assume in this paper that the detection function $K(x - y)$ satisfies

$$K(x - y) > 0,\ K(x - y) = K(y - x),\ \int_\Omega K(x - y)dy = 1,\ x, y \in \Omega. \tag{1.4}$$

This condition ensures that the spatially homogeneous steady states of (1.3) are the same as the corresponding system with local perception. If $K(x - y)$ is chosen as the Dirac delta function, i.e., $K(x - y) = \delta(x - y)$, then $h(x, t) = u(x, t)$ and (1.3) becomes the standard predator–prey model with prey-taxis (Wu et al. 2016; Jin and Wang 2017; Wang et al. 2021; Wang and Wang 2021). We will explore the influence of the detection functions on the stability of (1.3) and expect the generation of spatially inhomogeneous distributions with spatially periodic scenarios at bifurcations.

The remaining paper is organized as follows. In Sect. 2, we introduce some preliminary results on the well-posedness of solutions. In Sect. 3, we investigate the stability and instability of the spatially homogeneous steady states for different detection functions in either the finite or infinite domain. In Sect. 4, we apply the theoretical results

of Sect. 3 to investigate the dynamics of the consumer-resource model with nonlocal resource perception and Holling type-II functional response. We summarize our paper with discussion in Sect. 5.

Throughout the paper, $\mathbb{N}$ represents the set of all positive integers, $\mathbb{N}_0 = \mathbb{N} \cup \{0\}$ represents the set of all nonnegative integers, $\mathbb{R}$ represents the set of all real numbers and $\mathbb{R}^+$ represents the set of all positive real numbers.

2 Well-Posedness of Solutions

In this section, we investigate the well-posedness (existence, uniqueness and positivity) of solutions to system (1.3). We assume that the initial condition $u_0 \in C^2(\bar{\Omega})$, $v_0 \in C^2(\bar{\Omega})$ and functions f, g in (1.3) satisfy the following conditions:

- (f_1) The function $f \in C^1([0,\infty] \times [0,\infty], \mathbb{R})$, $f(0,v) = 0$ for $v \geq 0$, and there exists $F : [0,\infty) \to \mathbb{R}$ and $M > 0$ such that $f(u,v) \leq F(u)$, and F satisfies $F(0) = 0$, $F(u) < 0$ for $u > M$.
- (g_1) The function $g \in C^1([0,\infty] \times [0,\infty], \mathbb{R})$, $g(u,0) = 0$ for $u \geq 0$, and there exist $K_1 > 0$, $K_2 > 0$ such that $g(u,v) \leq (K_1 + K_2 u)v$.

Proposition 2.1 *Suppose that $d_1 > 0$, $d_2 > 0$, $\alpha \geq 0$ and f, g satisfy, (f_1), (g_1), respectively. Then, when $\Omega = (-\infty, +\infty)$ or $\Omega = (0, \ell\pi)$, system (1.3) with the initial condition $u_0 \in C^2(\bar{\Omega})$, $v_0 \in C^2(\bar{\Omega})$ possesses a unique solution $(u(x,t), v(x,t))$ for $(x,t) \in \bar{\Omega} \times [0,\infty)$, and $u, v \in C^{2,1}(\bar{\Omega} \times [0,\infty))$ if the detection function K satisfies*

(H_1): $\int_\Omega (\int_\Omega \partial_x K(x-y)dy)^p dx < +\infty$, *for all* $p > 1$

and the boundary conditions satisfy $Bu = a(x)u + b(x)u_x = Bv = a(x)v + b(x)v_x = 0$ with $a(x), b(x) \in C([0, \ell\pi])$. Moreover, if $u_0(x) > 0$ for $x \in \bar{\Omega}$, $v_0(x) \geq (\not\equiv) 0$ for $x \in \bar{\Omega}$, then $u(x,t) > 0$, $v(x,t) > 0$ for $(x,t) \in \bar{\Omega} \times [0,\infty)$.

Proof Define

$$
\begin{aligned}
&h_0(x) = \int_\Omega K(x-y)u_0(y)dy,\\
&F^{(1)}(t,x,u,v) = f(u(x,t), v(x,t)),\\
&F^{(2)}(t,x,u,v) = \alpha(v(x,t)(h_0)_x)_x + g(u(x,t), v(x,t)),
\end{aligned}
$$

then it follows from (f_1), (g_1) and (H_1) that $F^{(1)}$ and $F^{(2)}$ are continuous and there exist $\theta \in (0,1)$ and $L > 0$ satisfying

$$
\begin{aligned}
&|F^{(i)}(t,x,u_1,v_1) - F^{(i)}(s,x,u_2,v_2)|\\
&\quad \leq L(|t-s|^\theta + ||u_1 - u_2||_{C^1} + ||v_1 - v_2||_{C^1}), \quad i = 1,2.
\end{aligned}
$$

Thus, $F^{(i)}(i = 1,2)$ satisfies a Hölder condition with respect to t, and a Lipschitz condition with respect to u and v. It follows from Lunardi (1995, Proposition 7.3.3) that u, v can be solved uniquely on $t \in [0, \delta]$ for some $\delta > 0$. The condition (f_1)

guarantees that $u(x,t)$ is also bounded on $[0,\delta]$ by a constant $B_0 > 0$, see, e.g., Alikakos (1979, Theorem 3.1). According to (g_1), $v(x,t)$ satisfies

$$\begin{cases} v_t(x,t) \le d_2 v_{xx}(x,t) - \alpha(v(x,t)(h_0)_x)_x + (K_1 + K_2 B_0)v, & x \in \Omega,\ 0 < t < \delta, \\ v(x,0) = v_0(x), & x \in \Omega, \end{cases}$$

then $v(x,t)$ can also be bounded on $[0,\delta]$ from Alikakos (1979, Theorem 3.1). Repeating this process the solution can be extended to $[\delta, 2\delta]$ and further to $[k\delta, (k+1)\delta]$ for any $k \in \mathbb{N}$ in 1D finite or infinite domain Ω. Moreover from the maximum principle, $u(x,t) > 0$ and $v(x,t) > 0$ for $(x,t) \in \bar{\Omega} \times [0,\infty)$. □

Remark 2.1 (1) It is worth mentioning that the diffusion matrix of system (1.3) is triangular, so the local existence of nonnegative solution of (1.3) can also be obtained by standard results such as Amann (1990, Theorem 0.1), which is similar to the case of local prey-taxis systems (Wang et al. 2017) or general chemotaxis systems (Winkler 2020). On the other hand, little is known for the global solvability for (1.3), while such results are known for the case of systems with local prey-taxis (Jin and Wang 2017). Following (Wu et al. 2016), as interaction functions and the kernel function satisfy (f_1), (g_1) and (H_1), a unique global solution of (1.3) can be uniformly bounded by a constant depending on initial values.

(2) The technical conditions (f_1), (g_1) guarantee the global existence of the solutions to (1.3). A typical form of f, g satisfying the conditions (f_1),(g_1) is $f(u,v) = u\left(1-\frac{u}{a}\right) - \frac{buv}{1+u}$, $g(u,v) = -cv + \frac{buv}{1+u}$, respectively. For this case, the condition (f_1) is satisfied by choosing $F(u) = u(1-\frac{u}{a})$, and the condition (g_1) is satisfied by choosing K_1 to be any positive number and $K_2 = b$.

3 Stability and Instability of Spatially Homogeneous Steady State

In this section, we investigate the stability and instability of spatially homogeneous steady state of (1.3) for different kernels in the finite or infinite domain. For this purpose, we first assume that $E_* = (u_*, v_*)$ is a spatially homogeneous (positive) steady state of (1.3). The linearized system of (1.3) at (u_*, v_*) is

$$\begin{pmatrix} u_t \\ v_t \end{pmatrix} = D_1 \begin{pmatrix} u_{xx} \\ v_{xx} \end{pmatrix} + D_2 \begin{pmatrix} h_{xx} \\ 0 \end{pmatrix} + A \begin{pmatrix} u \\ v \end{pmatrix}, \tag{3.1}$$

where

$$D_1 = \begin{pmatrix} d_1 & 0 \\ 0 & d_2 \end{pmatrix},\ D_2 = \begin{pmatrix} 0 & 0 \\ -\alpha v_* & 0 \end{pmatrix},\ A = \begin{pmatrix} a_{11} & a_{12} \\ a_{21} & a_{22} \end{pmatrix}, \tag{3.2}$$

and

$$a_{11} = \frac{\partial f(u_*, v_*)}{\partial u},\ a_{12} = \frac{\partial f(u_*, v_*)}{\partial v},\ a_{21} = \frac{\partial g(u_*, v_*)}{\partial u},\ a_{22} = \frac{\partial g(u_*, v_*)}{\partial v}.$$

For the biological relevance of a consumer-resource model, throughout the paper, we always assume that

$$a_{12} < 0, \quad a_{21} > 0. \tag{C_1}$$

This implies that u is the resource and v is the consumer in (1.3). We further assume that without the perceptual movement ($\alpha = 0$), (u_*, v_*) is stable, i.e., the following conditions

$$\mathrm{Tr}(A) < 0, \quad \mathrm{Det}(A) > 0 \tag{C_2}$$

and

$$d_1 a_{22} + d_2 a_{11} < 2\sqrt{d_1 d_2 \mathrm{Det}(A)} \tag{C_3}$$

hold.

In what follows, we always assume $\alpha > 0$ and investigate the influence of the perceptual movement rate α and the detection function on the stability of the steady state E_* of (1.3) in both finite and infinite domains.

3.1 Finite Domain Case

Assume that the finite domain $\Omega = (0, \ell\pi)$ and the problem (1.3) is subject to the no-flux boundary condition

$$u_x(0, t) = u_x(\ell\pi, t) = 0. \tag{3.3}$$

For the finite domain, one of the commonly used detection functions is the spatial average $K(x - y) = \frac{1}{\ell\pi}$ (Furter and Grinfeld 1989). This spatial average detection function is often induced by the nonlocal crowding effect in the population dynamics, and its influence on the spatiotemporal dynamics of the population dynamics has been investigated in Chen and Yu (2018), Wu and Song (2019), Song et al. (2019), Shi et al. (2021). However, for the forager's resource perception function with this kind of detection function, $h(x, t) = \frac{1}{\ell\pi}\int_0^{\ell\pi} u(y, t)dy$ is independent of the spatial variable x. Thus, $h_x = 0$, which implies that the perceptual diffusion term $-\alpha(vh_x)_x$ in (1.3) vanishes. This implies that the spatial average detection function does not affect any dynamics of (1.3).

For the finite domain, another commonly used detection function is the Green function of the operator $-d_3\frac{\partial^2}{\partial x^2} + I$ with Neumann boundary condition (Ni et al. 2018), i.e., $K(x - y)$ is the solution of

$$\begin{cases} -d_3\frac{\partial^2 K}{\partial x^2} + K = \delta(x - y), \quad x \in (0, \ell\pi), \\ K_x(0 - y) = K_x(\ell\pi - y) = 0. \end{cases} \tag{3.4}$$

The Green function $K(x-y)$ is a monotonically decreasing function of $|x-y|$ and is consistent with the fact that the consumers have stronger perceptual to the resources nearby than those further away. For more biological interpretations of this kind of detection function, please refer to Gourley (2000), Ni et al. (2018).

It is easy from (3.4) and the symmetry of the Green function to verify that

$$\int_0^{\ell\pi} K(x-y)dy = \int_0^{\ell\pi} \delta(x-y)dx = 1. \tag{3.5}$$

Let $\phi_n(x) = \cos(nx/\ell)$ and define

$$L(\phi_n) = \int_0^{\ell\pi} K(x-y)\phi_n(y)dy.$$

Then, using integration by part and the boundary conditions in (3.4), we have

$$\begin{aligned} L(\phi_n(x)) &= \int_0^{\ell\pi} K(x-y)\cos\left(\frac{ny}{\ell}\right)dy \\ &= -\frac{1}{(n/\ell)^2}\int_0^{\ell\pi} K_{yy}(x-y)\cos\left(\frac{ny}{\ell}\right)dy \\ &= -\frac{1}{(n/\ell)^2}\int_0^{\ell\pi} \left(\frac{1}{d_3}K(x-y) - \frac{1}{d_3}\delta(y-x)\right)\cos\left(\frac{ny}{\ell}\right)dy \\ &= -\frac{1}{d_3(n/\ell)^2}L(\phi_n(x)) + \frac{1}{d_3(n/\ell)^2}\phi_n(x), \end{aligned}$$

which implies that

$$L(\phi_n(x)) = \frac{1}{1+d_3(n/\ell)^2}\phi_n(x). \tag{3.6}$$

Assume that (3.1) has the solution as follows:

$$\begin{pmatrix} u \\ v \end{pmatrix} = \begin{pmatrix} a_n \\ b_n \end{pmatrix} e^{\lambda_n t}\cos\left(\frac{nx}{\ell}\right), \tag{3.7}$$

which obviously satisfies the boundary condition (3.3) for $n \in \mathbb{N}_0$.

Letting $\sigma_n = (n/\ell)^2$, it is easy to verify that $\frac{\partial^2\phi_n(x)}{\partial x^2} = -\sigma_n\phi_n(x)$. Then, substituting (3.7) into (3.1) and noticing the orthogonality of the eigenfunctions $\cos(nx/\ell)$ and (3.6), one can conclude that if λ_n is the root of $\mathrm{Det}(\mathcal{M}_n(\lambda)) = 0$, then (3.7) is the solution of (1.3) subject to the boundary condition (3.3), where the characteristic matrix $\mathcal{M}_n(\lambda)$ is defined by

$$\mathcal{M}_n(\lambda) = \lambda I_2 + \sigma_n D_1 + \frac{\sigma_n}{1+d_3\sigma_n}D_2 - A. \tag{3.8}$$

Thus, if the detection function $K(x-y)$ is determined by (3.4), then the characteristic equation of (3.1) is

$$\Gamma_n(\lambda) = \mathrm{Det}\left(\mathcal{M}_n(\lambda)\right) = \lambda^2 - T_n\lambda + J_n(\alpha) = 0,\ n \in \mathbb{N}_0, \tag{3.9}$$

where

$$\begin{aligned} T_n &= \mathrm{Tr}(A) - \mathrm{Tr}(D_1)\sigma_n, \\ J_n(\alpha) &= d_1 d_2 \sigma_n^2 - (d_1 a_{22} + d_2 a_{11})\,\sigma_n + \mathrm{Det}(A) - \alpha a_{12} v_* \sigma_n H(\sigma_n), \end{aligned} \tag{3.10}$$

with

$$\mathrm{Tr}(A) = a_{11} + a_{22},\ \mathrm{Tr}(D_1) = d_1 + d_2,\ \mathrm{Det}(A) = a_{11}a_{22} - a_{12}a_{21},$$

and

$$H(\sigma_n) = \frac{1}{1 + d_3\sigma_n} > 0. \tag{3.11}$$

Under the conditions (C_2) and (C_3), it is easy to see from (3.10) that $T_n < 0$ and $J_n(0) > 0$. Furthermore, by the condition (C_1) and (3.11), we have $J_n(\alpha) > 0$ for any $\alpha \geq 0$. This implies that under the conditions (C_1), (C_2) and (C_3), all roots of Eq.(3.9) have negative real parts for any $n \in \mathbb{N}_0$ and $\alpha \geq 0$. Therefore, the steady state $E_* = (u_*, v_*)$ of (1.3) is asymptotically stable for the kernel function $K(x-y)$ defined by (3.4).

By the above discussion, we have the following results.

Theorem 3.1 *For system (1.3) subject to the no-flux boundary condition, assuming that the conditions (C_1), (C_2) and (C_3) hold, then E_* is always asymptotically stable for any $\alpha \geq 0$ regardless of whether the kernel is the spatial average or the Green's function defined by (3.4).*

3.2 Infinite Domain Case

For the infinite domain $\Omega = (-\infty, +\infty)$, we have

$$h(x,t) = \int_{-\infty}^{\infty} K(x-y)u(y,t)dy = \int_{-\infty}^{\infty} K(\xi)u(x-\xi,t)d\xi. \tag{3.12}$$

The following three widely used detection functions are considered (Ducrot et al. 2011; Fagan et al. 2017; Merchant and Nagata 2011):

1. Laplace: $K(x) = \frac{1}{2R}\exp(-|x|/R)$;
2. Gaussian: $K(x) = \frac{1}{\sqrt{2\pi}R}\exp(-x^2/2R^2)$;
3. Top-hat: $K(x) = \begin{cases} \frac{1}{2R} & -R \leq x \leq R, \\ 0, & otherwise. \end{cases}$

The Laplace and Gaussian detection functions allow the consumer to perceive nearby resources and decay monotonically as the increasing distance from the observation location. The top-hat detection function allows the consumer to perceive resources equally a fixed distance away from its current location and cannot detect beyond that fixed distance (Wang and Salmaniw 2023).

In the following, we investigate the influence of these three kinds of detection functions as above on the stability of the steady state $E_* = (u_*, v_*)$ and the possible bifurcation phenomenon.

Assume that (3.1) has the solution of the form

$$\begin{pmatrix} u \\ v \end{pmatrix} = \begin{pmatrix} a_k \\ b_k \end{pmatrix} e^{\lambda t + ikx}, \tag{3.13}$$

where $\lambda \in \mathbb{C}$ and $k \in \mathbb{R}$. Substituting (3.13) into (3.1), we obtain the characteristic equation

$$\Gamma_k(\lambda) = \lambda^2 - T_k\lambda + J_k(\alpha, R) = 0, \tag{3.14}$$

where

$$T_k = \mathrm{Tr}(A) - \mathrm{Tr}(D_1)k^2, \tag{3.15}$$

$$J_k(\alpha, R) = d_1 d_2 k^4 - (d_1 a_{22} + d_2 a_{11})\, k^2 + \mathrm{Det}(A) - \alpha a_{12} v_* k^2 H(R, k), \tag{3.16}$$

and

$$H(R,k) = \int_{-\infty}^{\infty} K(x) e^{-ikx} dx = \begin{cases} \frac{1}{1+R^2k^2} > 0, & \text{for Laplace detection function ,} \\ e^{-\frac{R^2k^2}{2}} > 0, & \text{for Gaussian detection function,} \end{cases} \tag{3.17}$$

and for the top-hat detection function,

$$\begin{aligned} H(R,k) &= \int_{-\infty}^{\infty} K(x) e^{-ikx} dx = \frac{1}{2R}\int_{-R}^{R} e^{-ikx} dx \\ &= \begin{cases} \frac{\sin(kR)}{kR}, & k \neq 0, \\ 1, & k = 0. \end{cases} \end{aligned} \tag{3.18}$$

3.2.1 Stability and Bifurcation Analysis for the Laplace and Gaussian Detection Functions

For the Laplace and Gaussian detection functions, we have the following results.

Theorem 3.2 *Assume that the conditions* (C_1), (C_2) *and* (C_3) *hold. For Gaussian and Laplacian detection functions, the steady state* E_* *of system (1.3) is always asymptotically stable for any* $\alpha > 0$ *and* $R \geq 0$.

Proof From the condition (C_2) and noticing the fact that T_k is independent of α and R, we $Tr(A) < 0$, which, together with (3.15), implies that for $\alpha > 0$ and $R \geq 0$, $T_k < 0$ for any $k \in \mathbb{R}$.

Under the conditions (C_2) and (C_3), it is easy to verify that $J_k(0, R) > 0$ for any $k \in \mathbb{R}$. It follows from (3.17) that for the Laplace kernel and Gaussian detection functions, $H(R, k) > 0$ for $R \geq 0$ and $k \in \mathbb{R}$. This, together with the condition (C_1) and $J_k(0, R) > 0$, implies that $J_k(\alpha, R) = J_k(0, R) - \alpha a_{12} v_* k^2 H(R, k) > 0$ for any $\alpha > 0$ and $R \geq 0$ since $a_{12} < 0$.

Therefore, under the conditions (C_1), (C_2) and (C_3), all roots of Eq.(3.9) have negative real parts for any $k \in \mathbb{R}$ when $\alpha > 0$ and $R \geq 0$. This means that Laplace kernel and Gaussian detection functions do not affect the stability of the steady state E_* of (1.3). The proof is completed. □

3.2.2 Stability and Bifurcation Analysis for the Top-Hat Detection Function

For the top-hat detection function, one can verify that

$$h(x, t) = \lim_{R \to 0^+} \int_\Omega K(x - y) u(y, t) dy = u(x, t).$$

In this sense, we can say that $R = 0$ corresponds to the local perception. In this case, $J_k(\alpha, 0)$ becomes

$$J_k(\alpha, 0) = J_k(0, 0) - \alpha a_{12} v_* k^2,$$

which yields $J_k(\alpha, 0) > 0$ for $k \in \mathbb{R}$ and $\alpha > 0$ under the conditions (C_1), (C_2) and (C_3). Therefore, the steady state E_* of system (1.3) with the local perception $(R = 0)$ is asymptotically stable.

In what follows, for the nonlocal top-hat detection function $(R > 0)$, we investigate the influence of the perceptual movement rate α and the detection scale R on the stability of the steady state E_* of (1.3). For this purpose, we need to investigate the distribution of roots of the characteristic equation (3.14) for $H(k, R)$ defined by (3.18). We first introduce the following two propositions, which are very useful for the investigation of the distribution of roots of (3.14).

Proposition 3.1 *Letting* $g_1(z) = -\sin(z)/z$ *and denoting the countable number of positive roots of the equation* $\tan(z) = z$ *by* $z_j > 0$*, we have the following properties on* $g_1(z)$*:*

(i) $g_1(z)$ *obtains its local maximum at* $z = z_j$, $j = 2(m - 1) + 1$ *and*

$$g_1(z_{2(m-1)+1}) > g_1(z_{2m+1}) > 0, \ m \in \mathbb{N};$$

(ii) $g_1(z)$ *obtains its local minimum at* $z = z_j$, $j = 2m$ *and*

$$g_1(z_{2m}) < g_1(z_{2(m+1)}) < 0, \ m \in \mathbb{N}.$$

Proof From $g_1(z) = -\sin(z)/z$, we have

$$\frac{dg_1(z)}{dz} = \frac{\sin(z) - z\cos(z)}{z^2}, \quad \frac{d^2g_1(z)}{dz^2} = \frac{z^2\sin(z) - 2(\sin(z) - z\cos(z))}{z^3}.$$

In terms of $\tan(z_j) = z_j$ as illustrated in Fig. 1, we have $0 < z_j < z_{j+1}$, $j = 1, 2, 3, \cdots$, and for $j = 2(m-1)+1$,

$$z_j \in \left(2(m-1)\pi + \pi,\ 2(m-1)\pi + \frac{3\pi}{2}\right),\ m \in \mathbb{N},$$

and for $j = 2m$,

$$z_j \in \left(2m\pi,\ 2m\pi + \frac{\pi}{2}\right),\ m \in \mathbb{N}.$$

Thus, we have

$$\left.\frac{dg_1(z)}{dz}\right|_{z=z_j} = 0, \quad \left.\frac{d^2g_1(z)}{dz^2}\right|_{z=z_j} = \frac{\sin(z_j)}{z_j} \begin{cases} < 0, & j = 2(m-1)+1, \\ > 0, & j = 2m, \end{cases}$$

which implies that $g_1(z)$ obtains its local maximum at $z = z_j$, $j = 2(m-1)+1$, and obtains its local minimum at $z = z_j$, $j = 2m$. Noticing that $1/z_j = \cos(z_j)/\sin(z_j)$, we have

$$g_1(z_{2(m-1)+1}) - g_1(z_{2m+1}) = \cos(z_{2m+1}) - \cos(z_{2(m-1)+1}). \tag{3.19}$$

By the property of z_j, we have

$$2m\pi + \frac{3\pi}{2} - z_{2m+1} < \left(2(m-1)\pi + \frac{3\pi}{2} - z_{2(m-1)+1}\right). \tag{3.20}$$

From (3.19), (3.20) and the monotone and periodicity of the cosine function, we conclude that

$$g_1(z_{2(m-1)+1}) > g_1(z_{2m+1}) > 0,\ m \in \mathbb{N}.$$

Similarly, we can prove that $g_1(z_{2m}) < g_1(z_{2(m+1)}) < 0,\ m \in \mathbb{N}$. The proof is completed. □

Noticing that for $k \neq 0$, $H(R, k) = H(R, -k)$, we only consider the case of $k > 0$ in what follows and define

$$f_1(k, R) = -\frac{\sin(kR)}{kR}. \tag{3.21}$$

Then, the following proposition follows immediately.

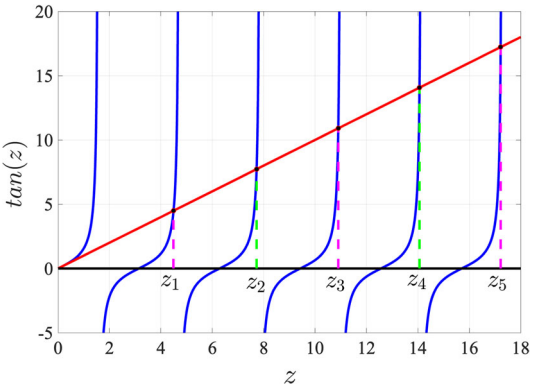

Fig. 1 The first five zeros z_j of $\tan(z) = z$. $z_1 \doteq 4.4869$, $z_2 \doteq 7.7250$, $z_3 \doteq 10.9041$, $z_4 \doteq 14.0657$, $z_5 \doteq 17.2201$

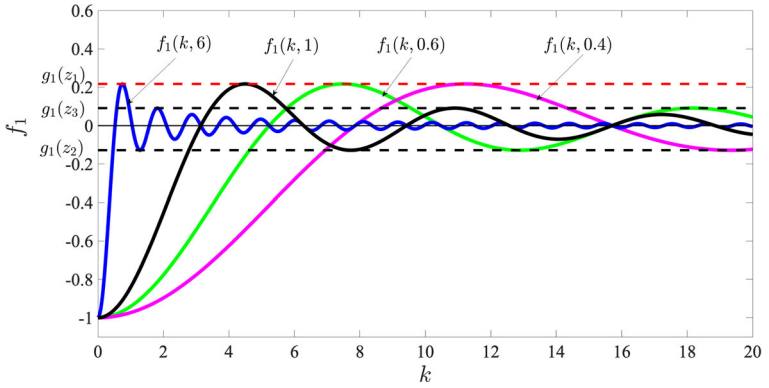

Fig. 2 The graphs of the function $f_1 = f_1(k, R)$ for $R = 6$, $R = 1$, $R = 0.6$ and $R = 0.4$. $g_j(z_j) = -\frac{\sin(z_j)}{z_j}$, $j = 1, 2, 3, 4$, where $z_1 \doteq 4.4869, z_2 \doteq 7.7250, z_3 \doteq 10.9041, z_4 \doteq 14.0657$. When R is decreasing, the curve $f_1 = f(k, R)$ stretches along the k-axis and the local extremums of the function $f_1 = f_1(k, R)$ keep unchanged, but the extremum point $(k_j, g_1(z_j))$ moves along the straight line $f_1 = -\frac{\sin(z_j)}{z_j}$

Proposition 3.2 *Assuming that z_j is defined by Proposition 3.1 and letting $k_j = z_j/R$, then we have the following results on the function $f_1(k, R)$ with R as the parameter:*

(i) for fixed R, the function $f_1 = f_1(k, R)$ obtains its local maximum $f(k_{2(m-1)+1}, R) = g_1(z_{2(m-1)+1}) > 0$ at $k = k_{2(m-1)+1}$, and obtains its local minimum $f(k_{2m}, R) = g_1(z_{2m}) < 0$ at $k = k_{2m}$, $m \in \mathbb{N}$;

(i) when R is increasing, the local extremum $f_1(k_j, R)$ of the function $f_1 = f_1(k, R)$ remains the same, but k_j is decreasing and $\lim\limits_{R\to 0} k_j = +\infty$, $\lim\limits_{R\to+\infty} k_j = 0$.

Figure 2 illustrates the graph of the function $f_1 = f_1(k, R)$ for different values of R and intuitively shows the results of Proposition (3.2).

Under the condition (C_2), it is easy to verify that $T_k < 0$ for any $k \in \mathbb{R}$. Thus, for fixed $k \in \mathbb{R}$, two roots of Eq. (3.14) have negative real parts for $J_k(\alpha, R) > 0$, Eq.(3.14) has one positive root and one negative root for $J_k(\alpha, R) < 0$ and Eq.(3.14) has zero

root and one negative root for $J_k(\alpha, R) = 0$. Taking α and R as bifurcation parameters, we have the following results on the distribution of roots of the characteristic equation (3.14).

Lemma 3.1 *Assume that the conditions* (C_1), (C_2) *and* (C_3) *hold, and let*

$$\alpha^{(m)} = \frac{\left(2\sqrt{d_1 d_2 \mathrm{Det}(A)} - (d_1 a_{22} + d_2 a_{11})\right) z_{2(m-1)+1}}{a_{12} v_* \sin(z_{2(m-1)+1})}, \ m \in \mathbb{N}. \tag{3.22}$$

For the characteristic equation (3.14) with the top-hat detection function, we have the following results.

(I) For $0 < \alpha < \alpha^{(1)}$, *all roots of Eq.(3.14) are negative for any* $k > 0$ *and any* $R > 0$.

(II) For $\alpha = \alpha^{(1)}$, *there exist a critical value* R_1^* *and a positive number* k_1^* *such that Eq.(3.14) has one zero root and one negative root at* $k = k_1^*$ *and all other roots are negative at* $k \neq k_1^*$ *for* $R = R_1^*$, *and all roots of Eq.(3.14) have negative real parts for any* $k > 0$ *and* $R \neq R_1^*$.

(III) For $\alpha^{(m)} < \alpha < \alpha^{(m+1)}, m \in \mathbb{N}$, *there exist two critical values* R_* *and* R^* *of* R *and two critical values* k_1^c *and* k_2^c *of* k *such that the curves* $f_1 = f_1(k, R)$ *and* $f_2 = f_2(k)$ *are tangent at* $(k, R) = (k_1^c, R_*)$ *or* $(k, R) = (k_2^c, R^*)$. *In this case, we have the following results:*

(1) if $R \in (0, R_*) \cup (R^*, +\infty)$, *then all roots of Eq.(3.14) are negative for any* $k > 0$; *and if* $R = R_*$, *then Eq.(3.14) has one zero root and one negative root at* $k = k_1^c$ *and all other roots are negative at* $k \neq k_1^c$; *and if* $R = R^*$, *then Eq.(3.14) has one zero root and one negative root at* $k = k_2^c$ *and all other roots are negative at* $k \neq k_2^c$;

(2) if $R \in (R_*, R^*)$, *then letting*

$$\begin{aligned}
I_R^+ &= \{R \,|\, R \in (R_*, R^*),\ f_1(k, R) < f_2(k) \text{ for } \forall k > 0\}, \\
I_R^- &= \left\{R \,\middle|\, R \in (R_*, R^*),\ \exists \text{ a set } k_s^- \subset \mathbb{R}^+,\ f_1(k, R) > f_2(k) \text{ for } k \in k_s^-\right\}, \\
I_R^0 &= \left\{R \,\middle|\, R \in (R_*, R^*),\ \exists \text{ a countable set } k_s^0 \subset \mathbb{R}^+,\right. \\
&\qquad \left. f_1(k, R) = f_2(k) \text{ for } k \in k_s^0,\ f_1(k, R) < f_2(k) \text{ for } k \notin k_s^0\right\},
\end{aligned}$$

there are the following two cases:

(i) for $I_R^+ = \emptyset$ *and* $I_R^0 = \emptyset$, *Eq.(3.14) has at least one positive root for* $k \in k_s^-$;

(ii) for $I_R^+ \neq \emptyset$, *all roots of Eq.(3.14) are negative for* $R \in I_R^+$, *and Eq.(3.14) has at least one positive root for* $k \in k_s^-$ *for* $R \in I_R^-$, *and Eq.(3.14) has zero roots for* $k \in k_s^0$ *and all other roots are negative for* $k \notin k_s^0$ *for* $R \in I_R^0$.

Proof From (3.16) and (3.18), it is easy to verify that $J_k(\alpha, R) > 0$ is equivalent to

$$-\frac{\sin(kR)}{kR} < \frac{1}{-\alpha a_{12} v_*}\left(d_1 d_2 k^2 + \frac{\mathrm{Det}(A)}{k^2} - (d_1 a_{22} + d_2 a_{11})\right). \tag{3.23}$$

Denote the function on the left-hand side of the inequality (3.23) by

$$f_1(k, R) = -\frac{\sin(kR)}{kR}, \tag{3.24}$$

and the function on the right-hand side of the inequality (3.23) by

$$f_2(k) = \frac{1}{-\alpha a_{12} v_*}\left(d_1 d_2 k^2 + \frac{\mathrm{Det}(A)}{k^2} - (d_1 a_{22} + d_2 a_{11})\right). \tag{3.25}$$

From the condition (C_3), it is easy to verify that

$$\begin{aligned} &d_1 d_2 k^2 + \frac{\mathrm{Det}(A)}{k^2} - (d_1 a_{22} + d_2 a_{11}) \\ &= \frac{1}{k^2}\left(d_1 d_2 k^4 - (d_1 a_{22} + d_2 a_{11}) k^2 + \mathrm{Det}(A)\right) > 0, \end{aligned}$$

which, together with the condition (C_1), implies that $f_2(k) > 0$. Noticing that $f_1(k, R)$ and $f_2(k)$ are both even functions with respect to k, we only need to consider the case of $k > 0$. From (3.25), we have

$$\frac{df_2(k)}{dk} = \frac{2}{-\alpha a_{12} v_*}\left(d_1 d_2 k - \frac{\mathrm{Det}(A)}{k^3}\right),$$

which implies that for fixed $\alpha > 0$, $f_2(k)$ is decreasing for $0 < k < k_c$ and increasing for $k > k_c$, where

$$k_c = \sqrt[4]{\frac{\mathrm{Det}(A)}{d_1 d_2}}.$$

Therefore, when $k > 0$, $f_2(k, \alpha)$ obtains its minimum

$$\min_{k>0}\{f_2(k)\} = f_2(k_c) = \frac{2\sqrt{d_1 d_2 \mathrm{Det}(A)} - (d_1 a_{22} + d_2 a_{11})}{-\alpha a_{12} v_*} > 0. \tag{3.26}$$

From the conditions (C_1) and (C_3), we have $a_{12} < 0$ and $2\sqrt{d_1 d_2 \mathrm{Det}(A)} - (d_1 a_{22} + d_2 a_{11}) > 0$, which implies that the minimum $f_2(k_c) > 0$.

Solving $g_1(z_{2(m-1)+1}) = f_2(k_c)$ for α, we have $\alpha = \alpha^{(m)}$ defined by (3.22). It is easy to see that $g_1(z_{2(m-1)+1}) > f_2(k_c)$ is equivalent to $\alpha > \alpha^{(m)}$.

By Proposition 3.1, we have

$$\max_{z>0}\{g_1(z)\} = g_1(z_1) = -\frac{\sin(z_1)}{z_1} > 0, \tag{3.27}$$

where $z_1 \in (\pi, 3\pi/2)$. Then, from (3.26) and (3.27), we can conclude that when $\alpha < \alpha^{(1)}$,

$$f_2(k_c) > \max_{z>0} \{g_1(z)\}. \tag{3.28}$$

In addition, from Proposition 3.2, it follows that

$$\max_{k>0} \{f_1(k, R)\} = g_1(z_1) = -\frac{\sin(z_1)}{z_1}. \tag{3.29}$$

From (3.28) and (3.29), we can conclude that for $\alpha < \alpha^{(1)}$,

$$f_2(k_c, \alpha) > \max_{k>0} \{f_1(k, R)\}, \tag{3.30}$$

which, together with the fact that the minimum $f_2(k_c)$ of the function $f_2(k)$ is increasing with the decreasing of α, implies that for $0 < \alpha < \alpha^{(1)}$, $f_2(k) > f_1(k, R)$ for $k > 0$ and any $R > 0$. This implies that for $\alpha < \alpha^{(1)}$, $J_k(\alpha, R) > 0$ for any $R > 0$. The conclusion (I) is confirmed.

It follows from Propositions 3.1 and 3.2 that $f(k, R)$ obtains its local extremum $g_1(z_j)$ at k_j, $g_1(z_j)$ is independent of R, but k_j is decreasing with the increasing of R and $\lim_{R\to+\infty} k_j = 0$ and $\lim_{R\to 0} k_j = +\infty$. This implies that when R is large enough or small enough, $f_1(k, R) < f_2(k)$ for any $k > 0$. In addition, noticing that with the increasing of R, the curve $f_1 = f(k, R)$ is compressed along the k-axis and the extremum point $(k_j, g_1(z_j))$ moves along the straight line $f_1 = g_1(z_j)$ from right to left.

Noticing that $g_1(z_1) = f_2(k_c, \alpha)$ for $\alpha = \alpha^{(1)}$. Therefore, when R is continuously changed from small enough to large, there must exist a critical value R_1^* and k_1^* such that the curves $f_1 = f_1(k, R_1^*)$ and $f_2 = f_2(k)$ are tangent at $k = k_1^*$ and $f_1(k, R_1^*) < f_2(k)$ for $k \neq k_1^*$. This proves the conclusion (II).

For $\alpha^{(m)} < \alpha < \alpha^{(m+1)}$, by the definition of $\alpha^{(m)}$, we have

$$g_1(z_{2(m-1)+1}) > \min_{k>0} \{f_2(k)\} = f_2(k_c, \alpha) > g_1(z_{2m+1}).$$

In addition, noticing that when R is small enough, $f_1(k, R) < f_2(k)$ for any $k > 0$, and the curve $f_1 = f_(k, R)$ is compressed along the k-axis with the increasing of R. Therefore, when R is changed from small to large, the curve $f_1 = f_1(k, R)$ must pass through the curve $f_2 = f_2(k)$ m times.

Denote the critical value of R by R_* such that when $R = R_*$, the curve $f_1 = f_1(k, R_*)$ is firstly tangent to the curve $f_2 = f_2(k)$ at $k = k_1^c$ and $f_2(k) > f_1(k, R_*)$ for $k \neq k_1^c$, as shown in Fig. 3 for $\alpha^{(1)} < \alpha < \alpha^{(2)}$. Then, we have

$$f_1(k_1^c, R_*) = f_2(k_1^c), \quad \frac{\partial f_1(k_1^c, R_*)}{\partial k} = f_2'(k_1^c), \quad \pi < k_1^c R_* < z_1.$$

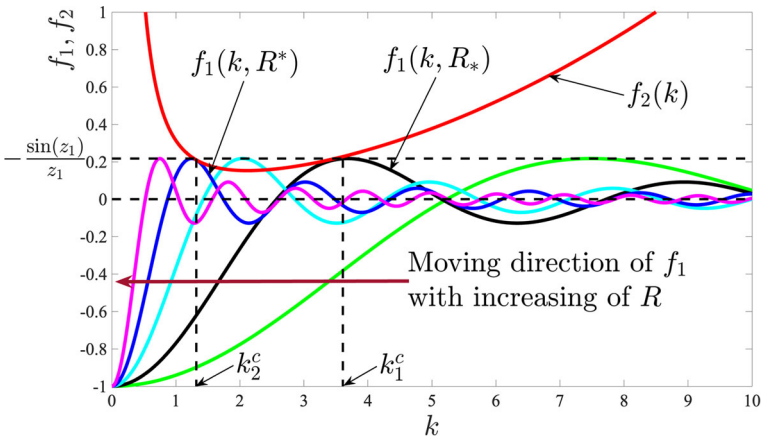

Fig. 3 The curves $f_1 = f_1(k, R)$ for different values of R, and $f_2 = f_2(k)$ for $a_{11} = -0.25, a_{12} = -1.6, a_{21} = 0.25, a_{22} = 0, d_1 = 0.1, d_2 = 0.2$ and $\alpha^{(1)} < \alpha = 3 < \alpha^{(2)}$. The curve $f_2 = f_2(k)$ is independent of R and the curve $f_1 = f_1(k, R)$ changes its shape as R varies. The first root of $f_1(k, R)$ is decreasing as R increases. The local minima and maxima of $f_1 = f_1(k, R)$ are independent of the R value. Here $R_* = 1.2196$, $R^* = 3.6090$, $z_1 \doteq 4.4869$ and $-\sin(z_1)/z_1 \doteq 0.2172$

Similarly, denote the critical value of R by R^* such that when $R = R^*$, the curve $f_1 = f_1(k, R^*)$ is finally tangent to the curve $f_2 = f_2(k)$ at $k = k_2^c$ and $f_2(k) > f_1(k, R^*)$ for $k \neq k_2^c$. Then, we have

$$f_1(k_2^c, R^*) = f_2(k_2^c), \ \frac{\partial f_1(k_2^c, R^*)}{\partial k} = f_2'(k_2^c), \ z_{2(m-1)+1} < k_2^c R^* < 2m\pi.$$

Therefore, if $R \in (0, R_*) \cup (R^*, +\infty)$, then $f_1(k, R) < f_2(k)$ for any $k > 0$. This confirms the conclusion $(III)(1)$.

For the case of $\alpha^{(m)} < \alpha < \alpha^{(m+1)}$ and $R \in (R_*, R^*)$, when either $R > R_*$ and close to R_* enough, or $R < R^*$ and close to R^* enough, there exist some $k > 0$ such that $f_1(k, R) > f_2(k)$. Therefore, when either $R > R_*$ and close to R_* enough, or $R < R^*$ and close to R^* enough, Eq.(3.14) has at least one positive root. However, if $R \in (R_*, R^*)$ and far from R_* and R^* such that $f_1(k, R) < f_2(k)$ for any $k > 0$, then all roots of Eq.(3.14) are negative for any $k > 0$. Then, by the definitions of I_R^+, I_R^- and I_R^0, the conclusion $(III)(2)$ follows immediately. □

Remark 3.1 For $\alpha^{(1)} < \alpha < \alpha^{(2)}$, it is easy to see that $I_R^+ = \emptyset$ and $I_R^0 = \emptyset$. Therefore, in this case, the characteristic equation (3.14) has at least one positive root for any $R \in (R_*, R^*)$.

Then, by Lemma (3.1) and Remark (3.1), we have the following theorem on the stability of the positive steady state E_* of system (1.3).

Theorem 3.3 *Assume that the conditions (C_1), (C_2) and (C_3) hold, and $\alpha^{(m)}$ is defined by (3.22). For system (1.3) with the top-hat detection function,*

(I) when $0 \le \alpha < \alpha^{(1)}$, E_* *is asymptotically stable for any* $R \ge 0$;
(II) when $\alpha > \alpha^{(1)}$, *we have the following results:*

(1) there exist two critical values R_* *and* R^* *of* R *such that system (1.3) undergoes Turing bifurcations at both* $R = R_*$ *and* $R = R^*$, *and* E_* *is asymptotically stable for* $R \in [0, R_*) \cup (R^*, +\infty)$;
(2) if $\alpha^{(1)} < \alpha < \alpha^{(2)}$, *then* E_* *is unstable for* $R \in (R_*, R^*)$;
(3) if $\alpha^{(m)} < \alpha < \alpha^{(m+1)}$ *with* $m \ge 2$ *and* $m \in \mathbb{N}$, *then there are the following two cases:*
(i) for $I_R^+ = \emptyset$ *and* $I_R^0 = \emptyset$, E_* *is unstable for* $R \in (R_*, R^*)$;
(ii) for $I_R^+ \ne \emptyset$, E_* *is asymptotically stable for* $R \in I_R^+$ *and unstable for* $R \in I_R^-$, *and system (1.3) undergoes Turing bifurcation for* $R \in I_R^0$.

If $\alpha > \alpha^{(1)}$ and the other parameters are fixed, the critical values R_* and R^* can be considered as the function of α denoted by $R_*(\alpha)$ and $R^*(\alpha)$. It follows from (3.26) that the minimum of $f_2(k)$ is decreasing as α increases. Therefore, by the proof of Lem 3.1, the following results on the monotonicity of $R^*(\alpha)$ and $R_*(\alpha)$ with respect to α follow immediately.

Theorem 3.4 *Assume that the conditions* (C_1), (C_2) *and* (C_3) *hold, and* $\alpha^{(m)}$ *is defined by (3.22). For system (1.3) with the top-hat detection function and* $\alpha > \alpha^{(1)}$, $R^*(\alpha)$ *is increasing and* $R_*(\alpha)$ *is decreasing as* α *increases.*

The corresponding ODE system of model (1.3) is

$$u' = f(u, v), \ v' = g(u, v). \tag{3.31}$$

It is easy to see that if $(\phi(t), \psi(t))$ is the solution of the ODE system (3.31), then $(u(x, t), v(x, t)) = (\phi(t), \psi(t))$ is the spatially homogeneous solution of system (1.3). Thus the Hopf bifurcating periodic solution of the ODE system (3.31) is the spatially homogeneous periodic solution of system (1.3). From this fact and Theorem 3.3, we obtain the following corollary.

Corollary 3.1 *Assume that the conditions* (C_1) *and* (C_3) *hold,* $Tr(A) \ge 0$ *and* $Det(A) > 0$. *If there exists a critical value* μ_h *of the parameter* μ *of the ODE system (3.31) such that system (3.31) undergoes Hopf bifurcation at* $\mu = \mu_h$, *then when* $\alpha > \alpha^{(1)}$, *system (1.3) with the top-hat detection function undergoes Turing–Hopf bifurcation at either* (μ_h, R_*) *or* (μ_h, R^*).

4 Application with Numerical Simulations

In this section, for the top-hat detection function, we illustrate how the detection scale R yields spatiotemporal patterns driven by the nonlocal resource perception as an application. We consider the following consumer-resource model with Holling type II functional response in the finite spatial domain $[-L, L]$ subject to periodic boundary

conditions:

$$\begin{cases} u_t = d_1 u_{xx} + u\left(1 - \dfrac{u}{a}\right) - \dfrac{buv}{1+u}, & -L < x < L,\ t > 0, \\ v_t = d_2 v_{xx} - \alpha(v h_x)_x - cv + \dfrac{buv}{1+u}, & -L < x < L,\ t > 0, \\ u(-L,t) = u(L,t),\ u_x(-L,t) = u_x(L,t),\ t > 0, \\ v(-L,t) = u(L,t),\ v_x(-L,t) = u_x(L,t),\ t > 0. \end{cases} \tag{4.1}$$

Here, we use the periodic boundary conditions because the periodic boundary conditions can be easily extend to the case of the infinite domain and it is easily operated in the numerical simulations. The periodic boundary conditions are often used in the literature for cognitive animal movement models (Wang and Salmaniw 2023; Giunta et al. 2021).

System (4.1) has a unique positive spatially homogeneous steady state $E_*(\gamma, v_\gamma)$, where

$$\gamma = \frac{c}{b-c}, \quad v_\gamma = \frac{(a-\gamma)(1+\gamma)}{ab},$$

provided that $b > c$ and $a > \frac{c}{b-c}$ hold. For this equilibrium $E_*(\gamma, v_\gamma)$, we have

$$\begin{aligned} a_{11} = \frac{\gamma(a-1-2\gamma)}{a(1+\gamma)} &\begin{cases} < 0, & \frac{c}{b-c} < a < 1 + \frac{2c}{b-c}, \\ > 0, & a > 1 + \frac{2c}{b-c}, \end{cases} \\ a_{12} = -c < 0, \quad a_{21} = \frac{a-\gamma}{a(1+\gamma)} &> 0, \quad a_{22} = 0. \end{aligned} \tag{4.2}$$

From (4.2), we can see that $Tr(A) = 0$ if and only if $a = a_h$, where

$$a_h = 1 + \frac{2c}{b-c}, \tag{4.3}$$

and when $\alpha = 0$, system (4.1) undergoes Hopf bifurcation at $a = a_h$, the spatially homogeneous steady state E_* is asymptotically stable when $b > c$ and $\frac{c}{b-c} < a < a_h$, and the Hopf bifurcating periodic solution for $a > a_h$ is stable (Yi et al. 2009). For any $a > a_h$, the corresponding ordinary differential system of (4.1) has a unique stable limit cycle (Cheng 1981; Hsu et al. 1978).

4.1 Influence of Nonlocal Resource Perception Range on Stability and Turing Patterns for $a < a_h$

When $b > c$ and $\frac{c}{b-c} < a < a_h$, we have $a_{11} < 0$ and then $d_1 a_{22} + d_2 a_{11} < 0$. Thus, the conditions (C_1), (C_2) and (C_3) hold. Thus, when $h(x,t) = u(x,t)$ (i.e., local resource perception), the spatially homogeneous steady state E_* of system (4.1) is linearly stable for any $d_1, d_2 \geq 0$ and $\alpha \geq 0$.

For numerical illustrations, we take the parameters as follows:

$$b = 3.2,\ c = 1.6,\ d_1 = 0.1,\ d_2 = 0.2. \tag{4.4}$$

Then we have $a_h = 3$. If we choose $a = 2 < a_h$, we have

$$u_* = 1,\ v_* = 0.3125,\ a_{11} = -0.25,\ a_{12} = -1.6,\ a_{21} = 0.25,\ a_{22} = 0.$$

In this case, there is no Hopf bifurcation since $a_{11} < 0$ and $a_{22} = 0$. The minimal positive root z_1 of the equation $\tan(z) = z$ is $z_1 \doteq 4.4869$, and $z_3 \doteq 10.9041$, $z_5 \doteq 17.2201$ (see Fig. 1). Then, by (3.22) we have

$$\alpha^{(1)} \doteq 2.1073,\ \alpha^{(2)} \doteq 5.0125,\ \alpha^{(3)} \doteq 7.8964.$$

Following Theorem 3.3, the positive steady state E_* is asymptotically stable for any $R \geq 0$ for $0 \leq \alpha < \alpha^{(1)}$, and the stability of E_* depends on the detection scale R for $\alpha > \alpha^{(1)}$.

Setting $\alpha^{(1)} \doteq 2.1073 < \alpha = 3 < \alpha^{(2)} \doteq 5.0125$, we have

$$f_2(k) = \frac{4}{15k^2} + \frac{k^2}{75} + \frac{1}{30}.$$

Letting

$$m(k, R) \triangleq f_2(k) - f_1(k, R) = \frac{4}{15k^2} + \frac{k^2}{75} + \frac{1}{30} + \frac{\sin(kR)}{kR},$$

we can see from (3.23) that $J(k, \alpha) > 0$ if and only if $m(k, R) > 0$. In the $k - R$ plane, the curve $m(k, R) = 0$ forms an island as shown in the left figure in Fig. 4. The critical values of R are $R_* = R_*(3) \doteq 1.2196$, $R^* = R^*(3) \doteq 3.6090$. The positive steady state E_* is asymptotically stable for $R \in [0, R_*) \cup (R^*, \infty)$ and becomes unstable with the emergence of spatiotemporal patterns for $R \in (R_*, R^*)$.

Similarly, for $\alpha^{(2)} \doteq 5.0125 < \alpha = 6 < \alpha^{(3)} \doteq 7.8964$, we have

$$f_2(k) = \frac{2}{15k^2} + \frac{k^2}{150} + \frac{1}{60},$$

and the curve $m(k, R) = 0$ forms two islands in the $k - R$ plane as shown in the right panel of Fig. 4, where

$$m(k, R) = \frac{2}{15k^2} + \frac{k^2}{150} + \frac{1}{60} + \frac{\sin(kR)}{kR}.$$

For this case, we have $R_* = R_*(6) \doteq 0.7945$, $R^* = R^*(6) \doteq 7.3135$.

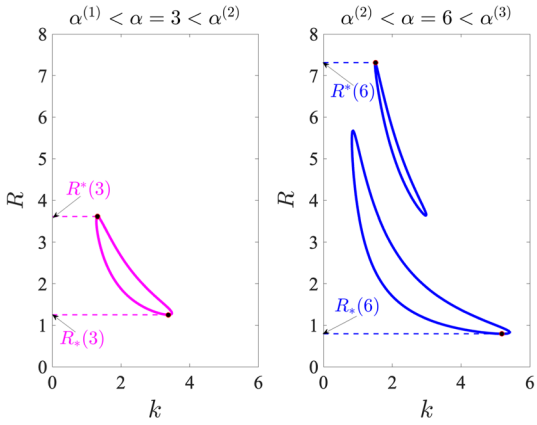

Fig. 4 The islands enclosed by $m(k, R) = 0$ for fixed α. $J_k(\alpha) < 0$ inside the islands and $J_k(\alpha) > 0$ outside the islands. Left panel: for $\alpha^{(1)} < \alpha = 3 < \alpha^{(2)}$, there is only one island and the critical values of R are $R_* = R_*(3) \doteq 1.2196$, $R^* = R^*(3) \doteq 3.6090$. Right panel: for $\alpha^{(2)} < \alpha = 6 < \alpha^{(3)}$, there is two islands and the critical values of R are $R_* = R_*(6) \doteq 0.7945$, $R^* = R^*(6) \doteq 7.3135$

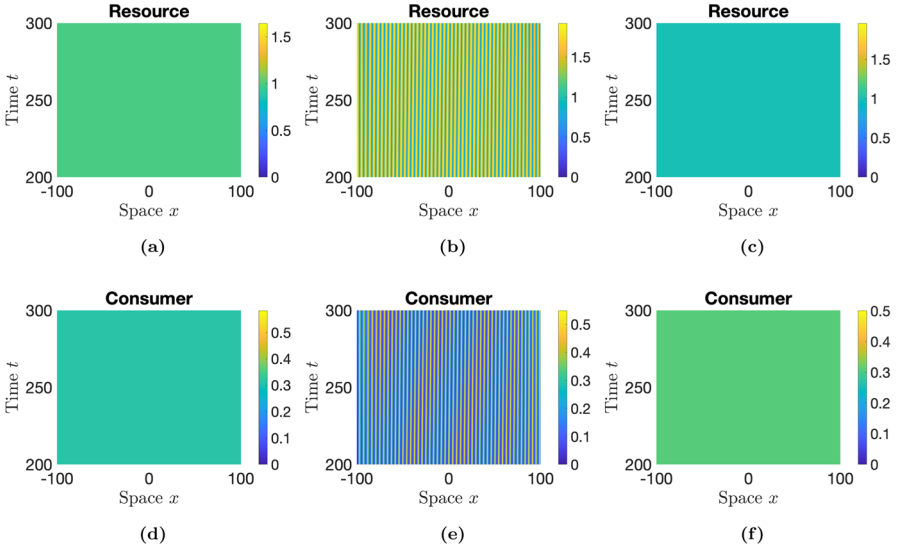

Fig. 5 Numerical simulations for different values of R for system (4.1) with $a = 2, \alpha = 3 \in \left(\alpha^{(1)}, \alpha^{(2)}\right)$ and other parameters as in (4.4). (a)(d) $R = 1.1 < R_* \doteq 1.2196$; (b)(e) $R = 3 \in \left(R_*, R^*\right)$; (c)(f) $R = 3.8 > R^* \doteq 3.6096$

For all numerical simulations, we choose $L = 100$ and consider the following initial conditions

$$u(x,0) = \begin{cases} 1, & |x| \le 50, \\ 0, & elsewhere, \end{cases} \qquad v(x,0) = \begin{cases} 0.3, & |x| \le 50, \\ 0, & elsewhere. \end{cases}$$

For $\alpha = 3 \in \left(\alpha^{(1)}, \alpha^{(2)}\right)$, Fig. 5 shows simulation results of system (4.1) for different values of R. Figure 5a and d illustrates the stability of E_* for $R = 1.1 < R_* \doteq 1.2196$. Figure 5c and f illustrates the stability of E_* for $R = 3.8 > R^* \doteq 3.6096$. Figure 5b and e illustrates Turing patterns for $R = 3 \in (R_*, R^*)$.

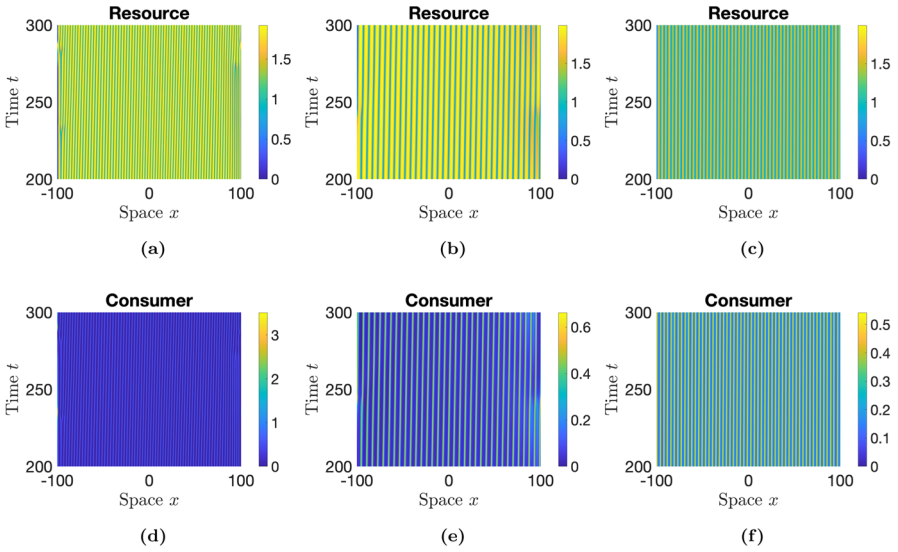

Fig. 6 Numerical simulations for different values of $R \in (R_*, R^*)$ for system (4.1) with $a = 2$, $\alpha = 6 \in (\alpha^{(2)}, \alpha^{(3)})$ and other parameters as in (4.4). For $\alpha = 6$, $R_* \doteq 0.7945$ and $R^* \doteq 7.3135$. (a)(d) $R = 2$; (b)(e) $R = 4.5$; (c)(f) $R = 6.5$

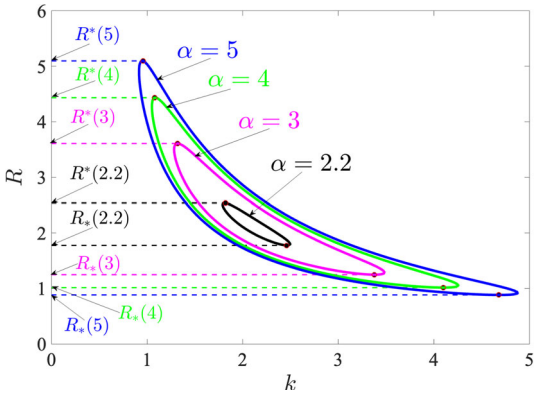

Fig. 7 The islands enclosed by $m(k, R) = 0$ for different values of $\alpha \in (\alpha^{(1)}, \alpha^{(2)})$. For fixed α, $J_k(\alpha) < 0$ inside the island and $J_k(\alpha) > 0$ outside the island. The critical value $R_*(\alpha)$ is decreasing as α increases, and $R^*(\alpha)$ is increasing as α increases

For $\alpha = 6 \in (\alpha^{(2)}, \alpha^{(3)})$, Fig. 6 shows the Turing patterns of system (4.1) for different values of $R \in (R_*, R^*)$. Figure 6(a)(d) illustrates the Turing patterns of system (4.1) for $R = 2$ larger than but close to R_*. Figure 6(b)(e) illustrates the Turing patterns of system (4.1) for $R = 4.5$ between and far away from both R_* and R^*. Figure 6(c)(f) illustrates the Turing patterns of system (4.1) for $R = 6.5$ smaller than but close to R^*. All these Turing patterns look like stripe patterns. From the right panel of Fig. 4, one can observe that the straight lines $R = 2$ and $R = 6.5$ cross one of the two islands, but the straight line $R = 4.5$ crosses both islands, and the width of the stripe patterns for $R = 4.5$ is larger than that of $R = 2$ or $R = 6.5$.

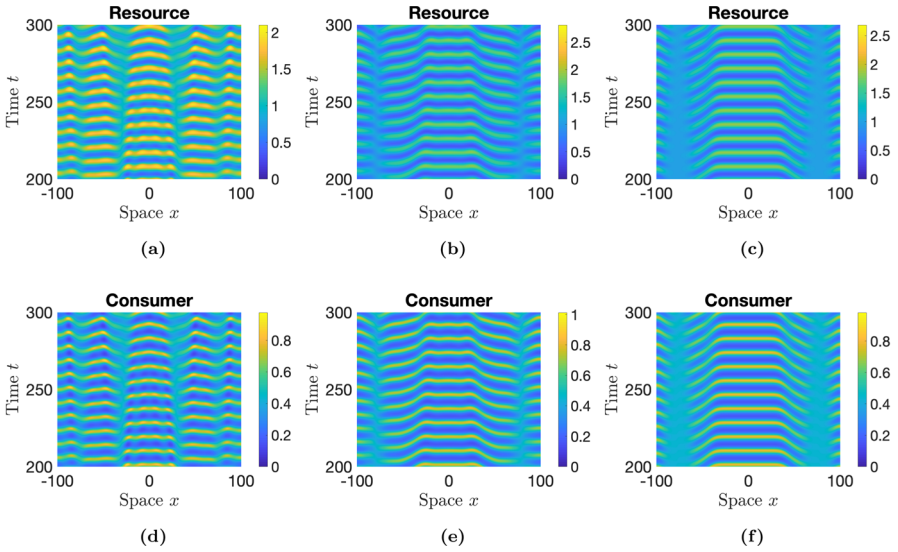

Fig. 8 Numerical simulations for system (4.1) with $\alpha = 0.8 < \alpha^{(1)}$, $a = 3.2 > a_h$ and other parameters given in (4.4). (a)(d) $R = 0.6$; (b)(e) $R = 7$; (c)(f) $R = 100$

Figure 7 illustrates the islands enclosed by the curve $m(k, R) = 0$ in the $k - R$ plane for different values of $\alpha \in \left(\alpha^{(1)}, \alpha^{(2)}\right)$. Figure 7 additionally shows that a bigger α leads to a larger island, which is in accordance with Theorem 3.4.

4.2 Spatiotemporal Patterns for $a > a_h$

4.2.1 Influence of Nonlocal Resource Perception Range on Spatiotemporal Patterns due to a Hopf Bifurcation

For fixed $a = 3.2 > a_h$ and other parameters b, c, d_1, d_2 same as in (4.4), we have $\alpha^{(1)} \doteq 1.3627$. It follows from the proof of Theorem 3.3 that for $\alpha < \alpha^{(1)} \doteq 1.3627$, there is no Turing bifurcation for any $R > 0$. Taking $\alpha = 0.8 < \alpha^{(1)}$, Fig. 8(a)(d), (b)(e) and (c)(f) illustrates the spatiotemporal patterns of system (4.1) for $R = 0.6$, $R = 7$ and $R = 100$, respectively. These numerical simulations show the existence of spatially inhomogeneous periodic solutions, and the spatial heterogeneity becomes weaker with the increase of resource perception range R.

4.2.2 Spatiotemporal Patterns due to the Interaction of Hopf and Turing Bifurcations

If we choose $a = a_h = 3$ and other parameters b, c, d_1, d_2 same as in (4.4), then it follows from (3.22) that

$$\alpha^{(1)} \doteq 1.4263, \ \alpha^{(2)} \doteq 3.3927, \ \alpha^{(3)} = 5.3447.$$

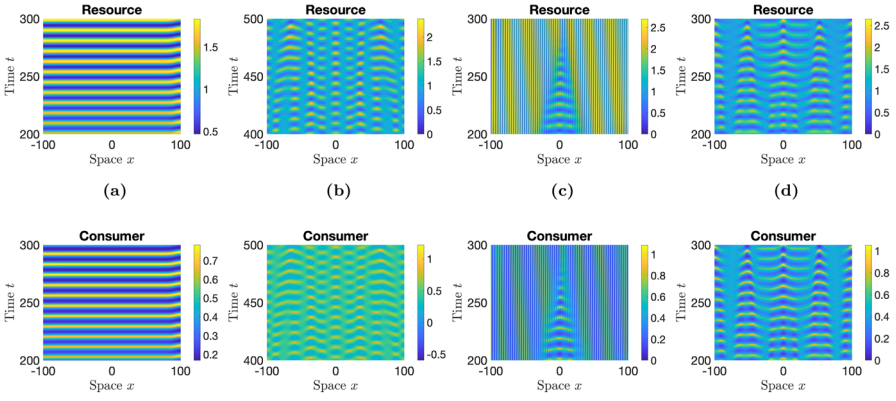

Fig. 9 Numerical simulations for system (4.1) for $a = 3.2 > a_h, \alpha = 1.5 \in \left(\alpha^{(1)}, \alpha^{(2)}\right)$. (a)(e): for system (4.1) with replacing $h(x,t)$ by $u(x,t)$ (equivalently, $R = 0$); (b)(f) $R = 0.15 < R_*$; (c)(g) $R = 2.31 \in \left(R_*, R^*\right)$; (d)(h) $R = 2.8 > R^*$

The proof of Lemma 3.1 implies that $J_k(\alpha) > 0$ for any $R > 0$ and $k \in \mathbb{R}$ when $\alpha < \alpha^{(1)} \doteq 1.4263$. Taking $\alpha = 1.5 \in \left(\alpha^{(1)}, \alpha^{(2)}\right)$, we have $R_* \doteq 1.6656$, $R^* \doteq 2.3536$. It follows from Corollary 3.1 that system (4.1) undergoes Turing–Hopf bifurcation at either $(a, R_*) \doteq (3, 1.6656)$ or $(a, R^*) \doteq (3, 2.3536)$. For fixed $a = 3.2 > a_h$, Fig. 9 illustrates how the spatiotemporal dynamics change as R increases. For system (4.1) with local perception ($h(x,t) = u(x,t)$, equivalently $R = 0$), Fig. 9(a)(e) shows the existence of spatially homogeneous periodic solution. For $R > 0$, the spatiotemporal dynamics is shown in Fig. 9(b)(f), (c)(g) and (d)(h), respectively, for $R = 0.15 < R_*$, $R = 2.31 \in (R_*, R^*)$ and $R = 2.8 > R^*$.

For fixed $a = 8$ far away from the Hopf bifurcation value a_h, Fig. 10 illustrates the evolution of the spatiotemporal dynamics of system (4.1) for $R = 4$, $R = 7$ and $R = 100$, respectively.

Finally, for fixed $\alpha = 3$ and $R = 10$, we numerically investigate the influence of maximum environmental capacity a on the spatiotemporal dynamics of system (4.1). Figure 11 illustrates the transition of the spatiotemporal dynamics of system (4.1) for $a = 3.5$, $a = 5$ and $a = 7$, respectively. These numerical simulations show the oscillatory patterns in time, and the oscillatory behavior and spatial heterogeneity become stronger as a increases. When a increases to 15, spatiotemporal chaos appears as shown in Fig. 12.

5 Discussion

In this paper, we investigate the spatiotemporal dynamics of cognitive consumer-resource dynamics with nonlocal perception. We focus on the impact of different detection functions on the stability of the spatially homogeneous steady state. We show that the nonlocal resource perception with top-hat detection function is one of the important mechanisms driving pattern formation. The investigation is performed

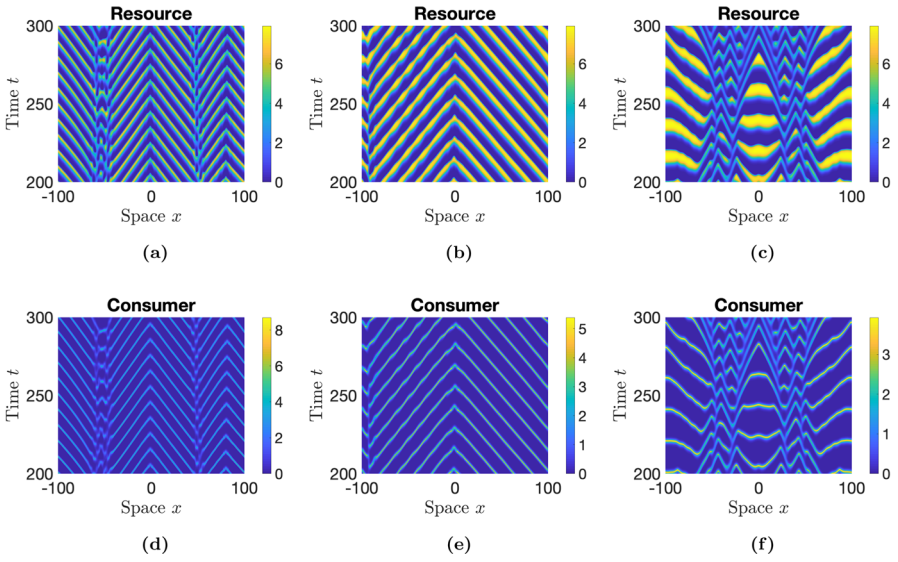

Fig. 10 Numerical simulations for system (4.1) with parameters given in (4.4), $a = 8$, and $\alpha = 1.5 \in \left(\alpha^{(1)}, \alpha^{(2)}\right)$. (a)(d) $R = 5$; (b)(e) $R = 7$; (c)(f) $R = 100$

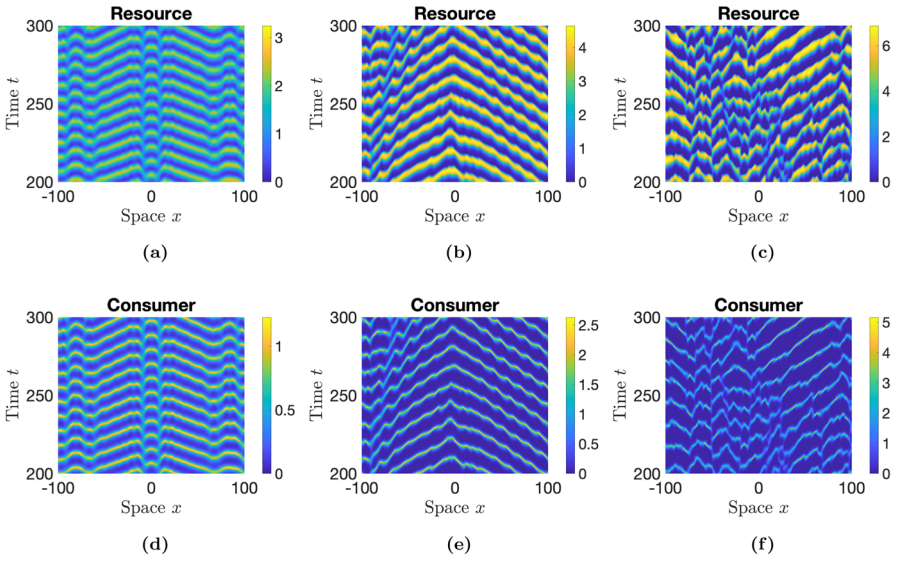

Fig. 11 Numerical simulations for system (4.1) for $\alpha = 3$ and $R = 10$. (a)(d) $a = 3.5$; (b)(e) $a = 5$; (c)(f) $a = 7$

for both finite and infinite domains. In the finite domain, the spatial average or Green function of the operator $-d_3 \frac{\partial^2}{\partial x^2} + I$ is chosen as the detection function to show that neither one affects the stability of the spatially homogeneous steady state. In the infinite domain, the Laplacian, Gaussian or top-hat detection function is considered

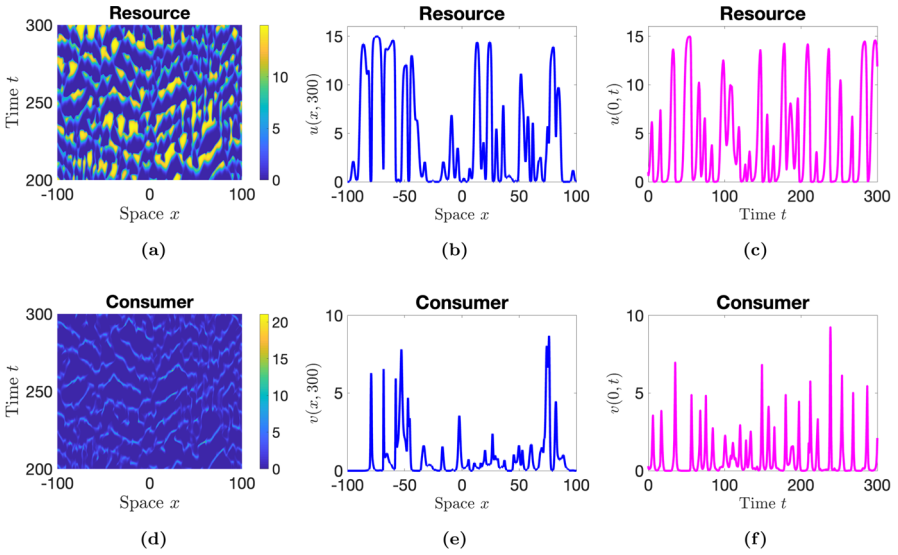

Fig. 12 Spatiotemporal chaotic patterns of resource (a) and consumer (d) for $\alpha = 3$, $R = 10$ and $a = 15$. (b)(e) are spatial distributions of resource and consumer, respectively, at time $t = 300$. (c)(f) are temporal evolution of resource and consumer, respectively, at location $x = 0$

for analysis. We prove that the first two detection functions have no influence on the stability of the spatially homogeneous steady state, but the top-hat detection function has significant influence on the stability.

For the top-hat detection function in the infinite domain, we investigate in detail the influence of the perceptual movement rate α and the detection scale R on the stability of the spatially homogeneous steady state. We find that when α is less than some threshold value $\alpha^{(1)}$, the spatially homogeneous steady state is always asymptotically stable no matter how large the detection scale R is. This implies that the nonlocal resource perception has no effect on the asymptotic dynamics of cognitive animal movement when the gradient-tracking movement is slow. However, when the perceptual movement rate is larger than the threshold value $\alpha^{(1)}$, the stability of the spatially homogeneous steady state depends on the detection scale. In this case, there exist two critical values R_* and R^* such that when the detection scale R is either smaller than R_* or larger than R^*, the spatially homogeneous steady state is asymptotically stable (see Fig. 5). From the biological perspective, it is reasonable to obtain the result that when the detection scale is small, the animal movement is the same as the local perception scenario. When the detection scale is large enough, the animal's perceptual movement follows a cognitive map. Although the stability of the spatially homogeneous steady state is consistent to the local perception scenario, the transient dynamics are expected to be quite different. The transient dynamics are mathematically more challenging but are worth a new development of rigorous methods. When the detection scale R is within the interval (R_*, R^*), the spatially homogeneous steady state loses its stability and a stable spatially inhomogeneous steady state emerges (see Fig. 6). This suggests that animals can better locate themselves in high resource places if they respond to

resources at intermediate perception ranges. This observation is not intuitively obvious and thus needs empirical evidence. The dependence of the critical values R_* and R^* on α is diagrammed in the k-R plane (see Fig. 7). R^* is increasing and R_* is decreasing with the increase of α. This implies that a faster gradient-tracking movement leads to a wider nonlocal detection range that causes spatially inhomogeneous distributions.

Theoretical results are employed to study a concrete consumer-resource model with Holling-II functional response and periodic boundary conditions. When the system with local resource perception has no Hopf bifurcation and the spatially homogeneous steady state is stable, the threshold values R_* and R^* of the detection scale are determined. For $R \in (R_*, R^*)$, stripe spatial patterns emerge.

When the corresponding ODE system undergoes Hopf bifurcation by taking the resource carrying capacity a as the bifurcation parameter and denoting the Hopf bifurcation value as a_h, we investigate the influence of the perceptual movement rate α and detection scale R on the spatiotemporal patterns. For $\alpha < \alpha^{(1)}$ and a larger than but close to a_h, the spatial heterogeneity becomes weaker with the detection scale R increases (see Fig. 8). The width of the top-hat kernel for the patterns near the origin of the spatial region is increasing as the detection scale R increases. Near the neighborhood of the Turing–Hopf bifurcation points (α_h, R_*) and (α_h, R_*), the spatiotemporal dynamics due to the interaction of Hopf bifurcation and Turing bifurcation are numerically investigated, and spatially inhomogeneous periodic patterns emerge (see Fig. 9). When $a > a_h$, as R increases from zero to a value greater than R^*, the spatiotemporal pattern switches from a spatially homogeneous periodic pattern, to spatially inhomogeneous periodic patterns, to a spatially inhomogeneous steady state, and eventually to spatially inhomogeneous periodic patterns. When a is far away from the Hopf bifurcation value a_h, oscillatory patterns with W-shaped and V-shaped spatial profiles emerge for different values of the detection scale R (see Fig. 10).

For a larger resource perception range, we investigate the influence of the resource carrying capacity a on the spatiotemporal dynamics. As the parameter a increases, the spatial heterogeneity becomes stronger (see Fig. 11) and the spatiotemporal patterns finally become spatiotemporal chaos (see Fig. 12). To validate this observation, empirical data need to be collected in resource-rich environments such as rainforests.

Acknowledgements The authors would like to thank the editor and the anonymous reviewers for their valuable comments and suggestions, which significantly improved the quality of our paper. Yongli Song's research was partially supported by grants from the Natural Science Foundation of Zhejiang Province (No.LZ23A010001) and the National Natural Science Foundation of China (No.12371166 and 11971143). Hao Wang's research was partially supported by grants from the Natural Sciences and Engineering Research Council of Canada (Discovery Grant RGPIN-2020-03911 and Accelerator Grant RGPAS-2020-00090) and the Canada Research Chairs program (Tier 1 Canada Research Chair Award). Jinfeng Wang's research was partially supported by a grant (No. 11971135) from the National Natural Science Foundation of China.

Author Contributions H.W. designed and supervised the research. Y.S. performed the research. J.W. wrote Section 2 Well-posedness of solutions. Y.S. and H.W. wrote the initial draft. All authors reviewed and edited the manuscript.

Declarations

Conflict of interest The authors declare no competing interests.

References

Alikakos, N.D.: L^p bounds of solutions of reaction-diffusion equations. Comm. Partial Differ. Equ. **4**(8), 827–868 (1979)

Amann, H.: Dynamic theory of quasilinear parabolic equations. II. Reaction-diffusion systems. Differ. Integral Equ. **3**(1), 13–75 (1990)

Barnett, A.H., Moorcroft, P.R.: Analytic steady-state space use patterns and rapid computations in mechanistic home range analysis. J. Math. Biol. **57**, 139–159 (2008)

Bellomo, N., Dogbé, C.: On the modeling of traffic and crowds: a survey of models, speculations, and perspectives. SIAM Rev. **53**, 409–463 (2011)

Börger, L., Dalziel, B.D., Fryxell, J.M.: Are there general mechanisms of animal home range behaviour? A review and prospects for future research. Ecol. Lett. **11**, 637–650 (2008)

Buttenschøn, A., Hillen, T.: Non-local cell adhesion models: symmetries and bifurcations in 1-D, vol. 1. Springer Nature, New York City (2021)

Carrillo, J.A., Chen, X., Wang, Q., Wang, Z., Zhang, L.: Phase transitions and bump solutions of the keller-segel model with volume exclusion. SIAM J. Appl. Math. **80**(1), 232–261 (2020)

Chen, L., Painter, K., Surulescu, C., Zhigun, A.: Mathematical models for cell migration: a non-local perspective. Philos. Trans. R. Soc. B **375**(1807), 20190379 (2020)

Chen, S., Yu, J.: Stability and bifurcation on predator-prey systems with nonlocal prey competition. Discret. Contin. Dyn. Syst. **38**(1), 43–62 (2018)

Cheng, K.S.: Uniqueness of a limit cycle for a predator-prey system. SIAM J. Math. Anal. **12**(4), 541–548 (1981)

Ducrot, A., Fu, X., Magal, P.: Turing and Turing-Hopf bifurcations for a reaction diffusion equation with nonlocal advection. J. Nonlinear Sci. **28**, 1959–1997 (2018)

Ducrot, A., Le Foll, F., Magal, P., Murakawa, H., Pasquier, J., Webb, G.F.: An in vitro cell population dynamics model incorporating cell size, quiescence, and contact inhibition. Math. Models Meth. Appl. Sci. **21**(1), 871–892 (2011)

Fagan, W.F., Gurarie, E., Bewick, S., Howard, A., Cantrell, R.S., Cosner, C.: Perceptual ranges, information gathering, and foraging success in dynamic landscapes. Am. Nat. **189**(5), 474–489 (2017)

Furter, J., Grinfeld, M.: Local vs. non-local interactions in population dynamics. J. Math. Biol. **27**(1), 65–80 (1989)

Giunta, V., Hillen, T., Lewis, M., Potts, J.R.: Local and global existence for non-local multi-species. SIAM J. Appl. Dyn. Syst. **21**(3), 1686–1708 (2021)

Gourley, S.A.: Travelling front solutions of a nonlocal Fisher equation. J. Math. Biol. **41**, 272–284 (2000)

Green, J.E.F., Waters, S.L., Whiteley, J.P., Edelstein-Keshet, L., Shakesheff, K.M., Byrne, H.M.: Non-local models for the formation of hepatocyte-stellate cell aggregates. J. Theor. Biol. **267**(1), 106–120 (2010)

Grünbaum, Daniel, Okubo, Akira: Modelling social animal aggregations, Frontiers in mathematical biology, Pages 296–325 in S. Levin, ed. ed., Springer, Berlin, (1994)

Hillen, T., Painter, K.J.: A user's guide to PDE models for chemotaxis. J. Math. Biol. **58**(1–2), 183–217 (2009)

Hsu, S.B., Hubbell, S.P., Waltman, P.: Competing predators. SIAM J. Appl. Math. **35**(4), 617–625 (1978)

Jin, H.-Y., Wang, Z.-A.: Global stability of prey-taxis systems. J. Differ. Equ. **262**(3), 1257–1290 (2017)

Keller, E.F., Segel, L.A.: Model for chemotaxis. J. Theor. Biol. **30**, 225–234 (1971)

Keller, E.F., Segel, L.A.: Traveling bands of chemotactic bacteria: a theoretical analysis. J. Theor. Biol. **30**, 377–380 (1971)

Lunardi, A.: Analytic semigroups and optimal regularity in parabolic problems. Progress in nonlinear differential equations and their applications, vol. 16. Birkhäuser Verlag, Basel (1995)

Martínez-García, R., Calabrese, J.M., Mueller, T., Olson, K.A., López, C.: Optimizing the search for resources by sharing information: Mongolian gazelles as a case study. Phys. Rev. Lett. **110**, 248–106 (2013)

Merchant, S., Nagata, W.: Instabilities and spatiotemporal patterns behind predator invasions with nonlocal prey competition. Theor. Popul. Biol. **80**(4), 289–297 (2011)

Mogilner, A., Edelstein-Keshet, L.: A non-local model for a swarm. J. Math. Biol. **38**, 534–570 (1999)

Ni, W., Shi, J., Wang, M.: Global stability and pattern formation in a nonlocal diffusive Lotka-Volterra competition model. J. Differ. Equ. **264**(11), 6891–6932 (2018)

Patlak, C.S.: Random walk with persistence and external bias. Bull. Math. Biophys. **15**, 311–338 (1953)

Shi, Q., Shi, J., Song, Y.: Effect of spatial average on the spatiotemporal pattern formation of reaction-diffusion systems. J. Dyn. Differ. Equ. **34**(3), 2123–2156 (2021)
Song, Y., Wu, S., Wang, H.: Spatiotemporal dynamics in the single population model with memory-based diffusion and nonlocal effect. J. Differ. Equ. **267**(11), 6316–6351 (2019)
Tao, Y., Winkler, M.: Boundedness in a quasilinear parabolic-parabolic Keller-Segel system with subcritical sensitivity. J. Differ. Equ. **252**, 692–715 (2012)
Tao, Y., Winkler, M.: Critical mass for infinite-time aggregation in a chemotaxis model with indirect signal production. J. Differ. Equ. **19**(12), 3641–3678 (2017)
Tao, Y., Winkler, M.: Effects of signal-dependent motilities in a Keller-Segel-type reaction-diffusion system. Math. Models Meth. Appl. Sci. **27**, 1645–1683 (2017)
Wang, G., Wang, J.: Pattern formation in predator prey systems with consuming resource and prey-taxis. Appl. Math. Lett. **111**, 106681 (2021)
Wang, H., Salmaniw, Y.: Open problems in pde models for knowledge-based animal movement via nonlocal perception and cognitive mapping, J. Math. Biol. **86**(5), (2023) https://doi.org/10.1007/s00285--023--01905--9
Wang, J., Wang, Z., Yang, W.: Uniqueness and convergence on equilibria of the Keller-Segel system with subcritical mass. Commun. Partial Differ. Equ. **44**(7), 545–572 (2019)
Wang, J., Wu, S., Shi, J.: Pattern formation in diffusive predator-prey systems with predator-taxis and prey-taxis. Discrete Contin. Dyn. Syst. Ser. B **26**(3), 1273–1289 (2021)
Wang, Q., Song, Y., Shao, L.: Nonconstant positive steady states and pattern formation of 1D prey-taxis systems. J. Nonlinear Sci. **27**(1), 71–97 (2017)
Winkler, M.: The role of superlinear damping in the construction of solutions to drift-diffusion problems with initial data in L^1. Adv. Nonlinear Anal. **9**(1), 526–566 (2020)
Wu, S., Shi, J., Wu, B.: Global existence of solutions and uniform persistence of a diffusive predator-prey model with prey-taxis. J. Differ. Equ. **260**(7), 5847–5874 (2016)
Wu, S., Song, Y.: Stability and spatiotemporal dynamics in a diffusive predator-prey model with nonlocal prey competition. Nonlinear Anal.-Real World Appl. **48**, 12–39 (2019)
Yi, F., Wei, J., Shi, J.: Bifurcation and spatiotemporal patterns in a homogeneous diffusive predator-prey system. J. Differ. Equ. **246**(5), 1944–1977 (2009)